Journal of Materials Chemistry C

PAPER

View Article Online
View Journal | View Issue



# Preparation and oxidation behavior of Ag-coated Cu nanoparticles less than 20 nm in size

Cite this: J. Mater. Chem. C, 2014, 2, 5372

Sang-Soo Chee[a] and Jong-Hyun Lee*[b]

Received 14th March 2014
Accepted 25th April 2014

DOI: 10.1039/c4tc00509k

www.rsc.org/MaterialsC

This study examines the oxidation behavior of Ag-coated Cu (Cu@Ag) nanoparticles (NPs) less than 20 nm in size synthesized using a solvothermal method and an immersion process with varying Ag shell quality. First, the mechanism for the formation of Cu NPs is discussed with respect to increasing reaction temperature and time. It was found that La Mer's model and the digestive-ripening mechanism affected the size and the morphology of the Cu NPs. Spherical Cu NPs were first observed after 15 min at 240 °C. Moreover, Cu@Ag NPs synthesized with varying immersion temperatures were observed by elemental mapping and line profile imaging using scanning transmission electron microscopy. The average thickness and density of the Ag shell increased with increasing immersion temperature. Based on the results, we evaluated the anti-oxidation property of samples immersed at 80 and 150 °C using high-temperature X-ray diffraction. The sample immersed at 150 °C exhibited an enhanced anti-oxidation property mainly as a result of the thicker and denser Ag shell. In particular, we observed a difference in the amount of free Ag NPs as a result of dewetting as the Ag shell structure changed. The anti-oxidation property of Cu@Ag NPs was strongly dependent on the Ag shell quality.

## 1. Introduction

Over the years, much research has been focused on the development of flexible and wearable devices such as flexible light-emitting diodes (LEDs),[1] flexible solar cells,[2–4] and batteries.[5–7] The preparation of flexible and wearable devices is compatible with diverse printing processes, and thus an expensive and complicated lithography process can be replaced by printing.[8–10] Ink-jet printing is a direct patterning method involving inks that contain nanoparticles (NPs).[9] It is fast and inexpensive; fine patterning of NPs can be formed just by printing, and patterned solid structures are completed by a subsequent sintering process. The technology has been widely applied to various fields such as radio-frequency identification (RFID) tags,[11,12] smart labels,[13] and electromagnetic interference (EMI) shielding.[14]

Ag NPs have been extensively used as conductive metal NPs because of their lower resistance as compared to other metal NPs.[15] However, Ag is an expensive metal, and its high material cost has caused a bottleneck in ink-jet printing technology. Cu NPs are an inexpensive alternative to Ag because their resistance is similar to that of Ag.[16,17] However, Cu NPs are vulnerable to surface oxidation in air.[17] To overcome the oxidation of Cu NPs, therefore, methods of fabricating Ag-coated Cu (Cu@Ag) NPs have been recently studied by many researchers.[18–21]

The Ag coating process can be classified under two methods: immersion[18–21]/electroless plating methods[22–24] and sonoelectrosynthesis.[25] The immersion plating process occurs by initiating a galvanic displacement reaction. This process is a very simple and convenient method. However, it is limited to Ag shells with thicknesses less than several nanometers, and it cannot be used on samples exposed to high temperatures, such as the front electrode of solar cells. Also, it has been reported that agglomerated Ag lumps tend to form on the Cu surface by Ag dewetting as a result of the unstable interfacial properties, thus inducing oxidation on the exposed pure Cu.[19,23]

The electroless plating method coats any type of material, including metals, ceramics and polymers. This process requires a reducing agent because there is no application of electrical energy. It is a fast process that results in a thicker coating as compared to immersion plating. Hai *et al.* reported that Cu@Ag powders with ~260 nm thick Ag shells were prepared using an electroless plating method.[22] However, the electroless plating method process could not be used to prepare a thin and uniform Ag coating on Cu NPs several tens of nanometers in size. It also induces Ag dewetting similar to that found in immersion-coated Cu@Ag NPs.[23] Accordingly, it will be important to analyze the Ag dewetting behavior in order to understand the usefulness of Cu@Ag NPs in conductive inks and to prevent the formation of Ag lumps and Cu oxidation, which can affect the conducting properties. Ultrafine Cu@Ag NPs smaller than 20 nm can be applied to ink-jet printing technology;

[a]Department of Materials Science & Engineering, Seoul National University of Science & Technology, Seoul 139-743, Republic of Korea
[b]Department of Materials Science & Engineering, Seoul National University of Science & Technology, Seoul 139-743, Republic of Korea. E-mail: pljh@snut.ac.kr

however, Ag dewetting of Cu@Ag NPs during sintering has not been discussed.

In this study, ultrafine Cu@Ag NPs smaller than 20 nm, which can be applied to ink-jet printing, were synthesized using a solvothermal method and an immersion-coating process, and the Ag dewetting behavior and Cu oxidation were analyzed. Also, the influence of quality of the Ag shell on Ag dewetting and Cu oxidation is discussed.

## 2. Experimental details

A solvothermal method was performed for 3 h at 230–250 °C to synthesize Cu NPs. Cu NPs formed using varying reaction temperatures and times were examined using transmission electron microscopy (TEM) and X-ray diffraction (XRD). Cu(II) acetyl acetonate ($Cu(C_5H_7O_2)_2$, $Cu(acac)_2$, 99.99%, Aldrich Co.) and oleylamine (OA, 70%, Aldrich Co.) were used as a Cu precursor and a solvent/reducing agent/capping agent, respectively. After optimal synthesis of the Cu NPs, an Ag immersion-coating process was conducted using varying temperatures. Silver nitrate ($AgNO_3$, 99.9%, Kojima Chemicals) was used as an Ag precursor for the Ag shell coating. After the Ag coating, OA was repetitively exchanged with ethanol (99.9%, Ducksan Chemical Co.) using a centrifuge in order to remove unnecessary ionic impurities and excess OA in the final NPs. All chemicals were used as-received without further processing or purification.

### 2.1. Synthesis of Cu nanoparticles by a solvothermal method

For synthesizing Cu NPs using a solvothermal method, 3.82 mM of $Cu(acac)_2$ was dissolved in 100 mL of OA for 30 min at 45 °C using a magnetic stirring bar. The synthesis in solution was performed under continuous $N_2$ bubbling to prepare pure Cu without forming oxide. After the complete dissolution, the solution was heated to and maintained at 240 °C for 3 h. The color of the solution changed from blue to reddish-brown at the end. This reddish-brown solution was cooled for 1 h. The solution containing NPs was centrifuged at 4000 rpm (67 $s^{-1}$) for 10 min and the medium was exchanged five times with ethanol to remove unnecessary ionic impurities and OA. Finally, the Cu NPs dispersed in ethanol were collected.

### 2.2. Synthesis of Cu@Ag core–shell nanoparticles using an immersion-coating process

After preparing pure Cu NPs, the Ag precursor was added to 30 mL of OA and allowed to dissolve for 1 h at 60 °C. The amount of Ag precursor added was determined based on the Cu/Ag atomic ratio of 4/1. The completely dissolved solution was then poured into the solution containing pure Cu NPs. This solution was heated for 2 h at different temperatures (80, 130, and 150 °C) under $N_2$ bubbling and stirring. Eventually, the color of the solution changed from reddish-brown to yellowish-red. This colloidal solution was cooled for 1 h at room temperature with continual stirring. It was then washed using ethanol *via* centrifugation at 10 000 rpm (167 $s^{-1}$) for 10 min several times. The Cu@Ag NPs dispersed in ethanol were then collected.

### 2.3. Characterization

X-ray diffraction (XRD, X'pert PRO-MPD, PANalytical) analysis was applied to confirm the crystal structure of Cu and to determine whether the Cu NPs were oxygenated or not. XRD was carried out in the $2\theta$ range of 20–80° using Cu K$\alpha$ radiation. To examine the morphologies of the Cu and Cu@Ag NPs, transmission electron microscopy (TEM, Tecnai $G^2$ F30ST, FEI Company) was performed at 300 kV. In addition, scanning transmission electron microscopy (STEM) was used to analyze the elemental distribution of Cu and Ag following the same conditions that were used in TEM.

The TEM and STEM analysis samples were prepared by adding a droplet of the ethanol solution containing either Cu or Cu@Ag NPs on a molybdenum grid. Also, OA-capped Cu NPs were investigated using Fourier transform infrared (FT-IR) spectroscopy (Vertex 80, Bruker Optics Co.) to identify the capping layer on the surface. The dried Cu NPs were additionally analyzed using differential scanning calorimetry (DSC, Q-20, TA Instruments) to identify the thermal characteristics. The signal was recorded from 50 °C to 275 °C at the rate of 3 °C $min^{-1}$ under a nitrogen gas flow (50 mL $min^{-1}$). High-temperature XRD (D/MAX 2200V/PC, Rigaku Co.) was performed to evaluate the anti-oxidation properties of Cu and Cu@Ag NPs.

## 3. Results

### 3.1. Characterization of Cu nanoparticles

Fig. 1 shows the TEM images of the synthesized Cu NPs at different reaction temperatures. The Cu NPs were not only non-uniform in size and morphology but also agglomerated after 3 h at 230 °C [Fig. 1(a)]. In the case of the sample synthesized for 3 h at 240 °C [Fig. 1(b)], the average size of the Cu NPs was estimated to be 11.60 nm ($\sigma \leq 1.98$ nm), and they showed enhanced mono-dispersity. Extremely fine (less than 10 nm) Cu NPs were obtained by synthesis for 3 h at 250 °C; the TEM image of the resulting particles is shown in Fig. 1(c). These results indicate that the solvothermal method used in this study is very simple and can be used to control the size and agglomeration degree of nanoscale Cu particles.

From the results shown in Fig. 1, it is believed that the optimal reaction temperature for synthesizing uniform and monodispersed Cu NPs is 240 °C. We therefore set the reaction temperature at 240 °C and varied the reaction times in order to observe the morphological transition of NPs as a function of increasing reaction time (Fig. 2). Extremely fine NPs were formed in 8 min and had estimated sizes below 10 nm. However, the NP size gradually increased to approximately 30 nm after 15 min. The NPs were initially polyhedrons, but they attained a spherical shape as the reaction time increased to 180 min. In addition, the dispersion and size uniformity was enhanced as a function of increasing reaction time. Thus, it was believed that the optimized condition to achieve uniform and

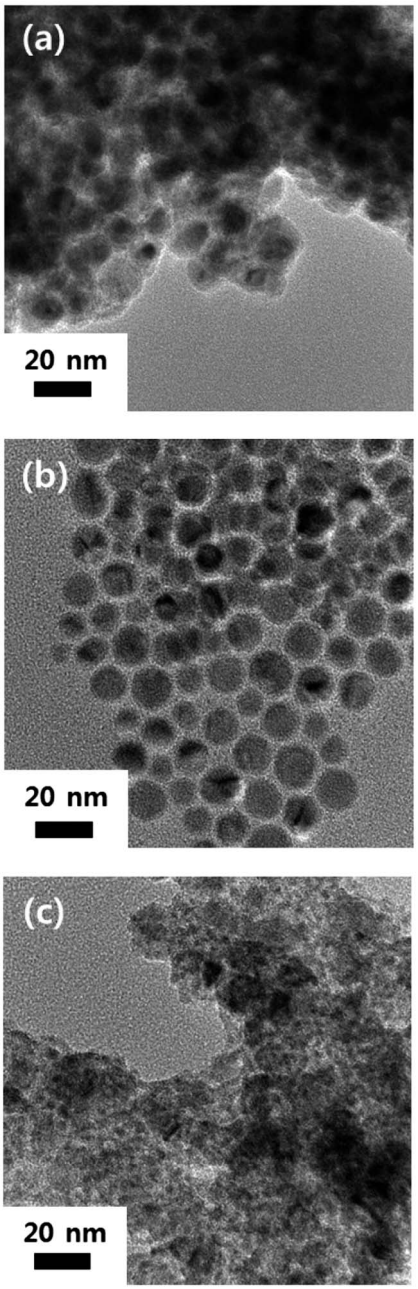


Fig. 1 TEM images of Cu NPs synthesized using a solvothermal method for 3 h at different reaction temperatures: (a) 230, (b) 240, and (c) 250 °C.

monodispersed NPs was a reaction time of 3 h at a temperature of 240 °C.

XRD was done to index the phase transformation with increasing reaction time, and the results of which are shown in Fig. 3. $Cu_2O$ was only observed in the initial 12 min at 240 °C, indicating that the NPs showing irregular morphologies in Fig. 2(a) and (b) were $Cu_2O$. A slight Cu(111) peak appears after heating for 15 min, which is when nearly spherical NPs were formed, which correlates with the TEM image of Fig. 2(c). As the reaction time increased, the intensity of the pure Cu peaks increased because of the increased reduction of Cu, implying that the spherical NPs consisted of a pure Cu phase. After the reaction had progressed for 1 h [Fig. 2(g)], almost all the NPs consisted of a pure Cu phase. Although weak intensities of $Cu_2O$ were observed in the all samples heated for more than 1 h, it is estimated that the $Cu_2O$ was formed by surface oxidation during the drying process of sample preparation. In summary, the aggregates of irregularly shaped ultrafine $Cu_2O$ NPs were consistently transformed into well-dispersed spherical Cu NPs with an average diameter of 11.60 nm as the reaction time increased up to 180 min.

Fig. 4 shows the FT-IR spectra and thermal analysis of the Cu NPs, which were carried out to confirm chemisorption on the surface and determine the recrystallization temperature. In the pure OA spectrum shown in Fig. 4(a), a N–H wagging group was observed at 650–900 $cm^{-1}$.[26] Moreover, the peaks at 909, 933, and 964 $cm^{-1}$ corresponded to the $NH_2$ bending group.[26,27] The peaks at 1042 $cm^{-1}$, 1468 $cm^{-1}$, 1568 $cm^{-1}$, 2860 $cm^{-1}$, 2930 $cm^{-1}$, and 3300 $cm^{-1}$ were applicable to the C–N stretching group,[26] C–H bending group,[26] $NH_2$ scissor group,[26] C–H stretching group,[26,27] and N–H stretching group,[27,28] respectively. Peaks indicating the N–H stretching group, C–H stretching group, C–H bending group, and C–N stretching group were identically detected in the OA-capped Cu NP peak, implying that OA was capped on the Cu NP surface.[28] However, the slight oxidation results observed in Fig. 3 indicate that the OA capping did not play a significant role in suppressing oxide formation on the Cu NPs.

The DSC results for the dried Cu NPs are shown in Fig. 4(b). The initial exothermal peak was observed at 115.93 °C during the first cycle, revealing that the crystallization of the Cu NPs was due to unstable crystals. Choi *et al.* reported that the initial crystallization exothermal peaks, depending on the particle size, were observed at 108 and 131 °C when Cu NPs approximately 9 and 17 nm in size, respectively, were synthesized.[29] As shown in Fig. 4(b), the first exothermal peak was observed at 115.93 °C in our experiment, indicating that the Cu NP size was 11–12 nm. This result correlated well with the TEM images in Fig. 1(b) and 2(h). The peak during the second cycle implied an exothermic reaction by thermal oxidation of Cu NPs. The initial point of significant oxidation under continuous heating at the rate of 3 °C $min^{-1}$ was 227.67 °C in both the first and second cycle. The oxidation is interpreted as being due to the effect of trace oxygen in the non-hermetically sealed system.

### 3.2. Characterization of Cu@Ag nanoparticles

Fig. 5 shows the TEM images and the selected area electron diffraction (SAED) pattern of Cu NPs immersed for 2 h at 80 °C in the Ag precursor. As compared to Cu NPs synthesized for 3 h at 240 °C [Fig. 1(b) and 2(h)], the average diameter of the Cu@Ag NPs increased by 3.46 nm. This value can be considered as roughly double the actual Ag shell thickness. The SAED pattern, shown in the inset of Fig. 5(b), was used to analyze the existence of an oxide layer on the Cu surface. As a result, only Cu and Ag crystal planes were observed, with no oxide layers. This confirms that the minor $Cu_2O$ phase observed in the 3 h-synthesis sample shown in Fig. 3 was formed during the

 

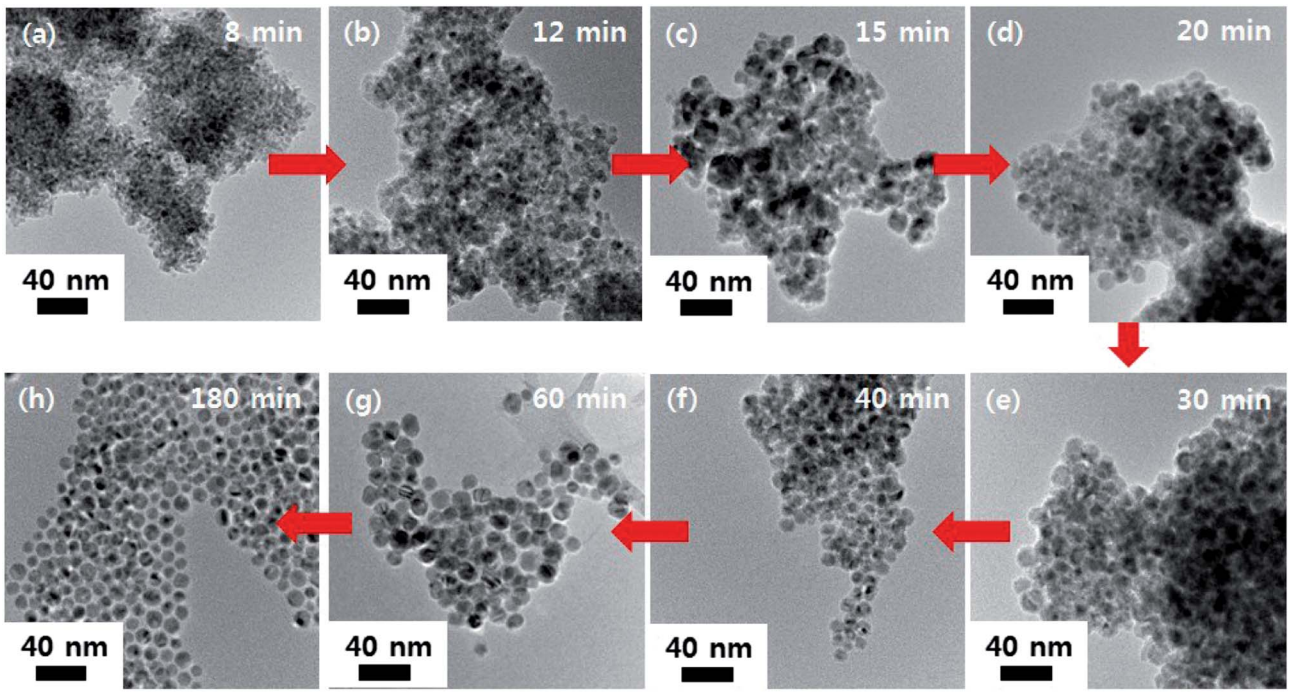


Fig. 2 TEM images of NPs as a function of reaction time in solvothermal synthesis at 240 °C.

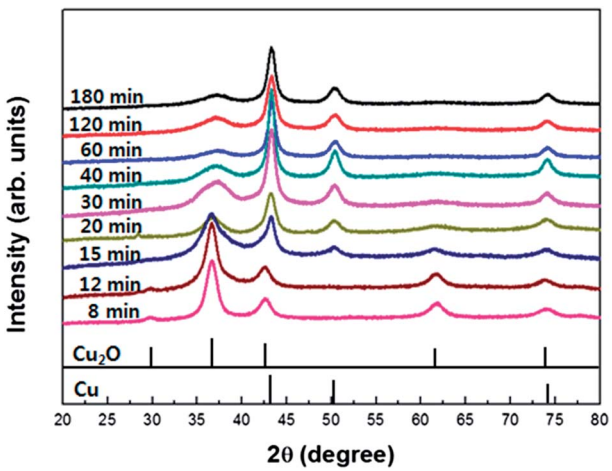


Fig. 3 XRD patterns of NPs with increasing reaction time.

drying process for TEM sampling and that the oxidation behavior could be suppressed when the Cu NPs were coated by Ag. However, the size of the Cu NPs ranged from 11 to 17 nm (average diameter: 15.06 nm), and the increased size deviation ($\sigma \leq 2.55$ nm) suggests that the Ag did not uniformly coat the Cu NPs, even after the addition of the Ag precursor for a sufficient duration.

The immersion temperature was increased to 130 and 150 °C in order to achieve sufficient and uniform deposition with the added Ag precursor, the results of which are shown in Fig. 6. At 130 and 150 °C, the Cu@Ag NP size was estimated to be approximately 16.49 ($\sigma \leq 1.96$) and 17.08 ($\sigma \leq 1.88$) nm, respectively, indicating increased size and decreased size deviation as compared to the result shown in Fig. 5. The average thickness and uniformity of the Ag shell increased because of the enhanced activation of galvanic displacement and deposition due to the increased immersion temperature. An Ag monolayer would initially form on the Cu NP surface *via* a galvanic displacement reaction. This was followed by additional deposition with the increasing immersion temperature. However, higher immersion temperatures might be harmful to the thickness and uniformity of the Ag shell. Jung *et al.* used a two-step method in the synthesis and size control experiments of Ag NPs, using nucleation for 1 h at 180 °C, and a holding step at 150 °C for NP growth.[30] Hence if this immersion solution is heated above 150 °C, the remaining Ag ions would not coat the Cu surface; instead, they would form Ag NPs through homogeneous nucleation.

To identify the element distribution in Cu@Ag NPs, STEM elemental mapping and line profile analysis were performed and the results are shown in Fig. 7. The core–shell structures were confirmed in all samples (80, 130, and 150 °C). The Ag shell thickness increased with increasing immersion temperature, as shown in the line profile images. Moreover, the Ag shell became gradually denser with increased immersion temperature, as shown in the elemental mapping images. These tendencies agree with those shown in Fig. 5 and 6. Consequently, the Ag shell quality was decided by the immersion temperature, and the Cu@Ag NPs treated at 150 °C were expected to be more effective in preventing Cu oxidation.

Fig. 8 shows XRD patterns of the dried Cu@Ag NPs as a function of different immersion coating temperatures. The samples did not contain a $Cu_2O$ phase, which indicates that the Ag coating was definitely helpful in preventing the surface

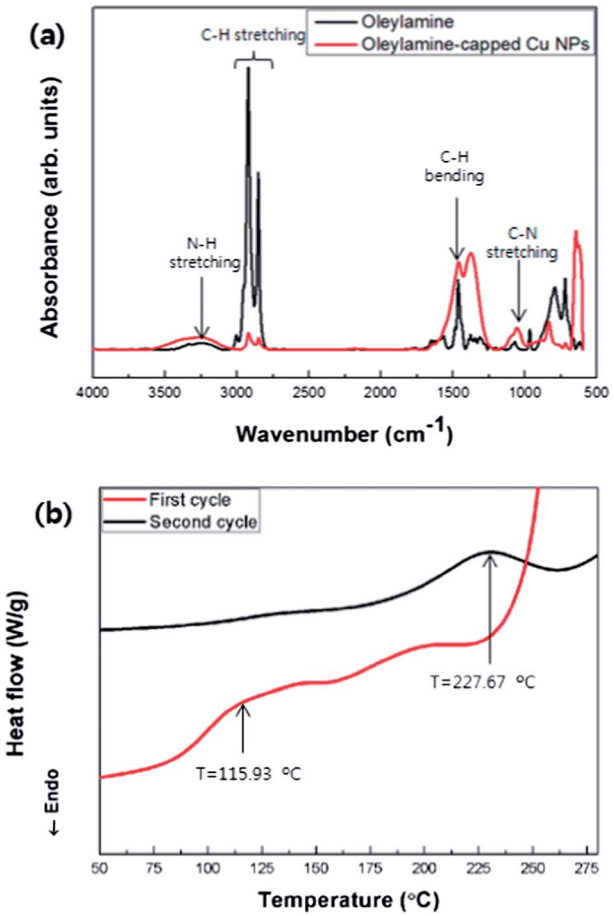


Fig. 4 (a) FT-IR spectra of Cu NPs synthesized using a solvothermal method with a pure oleylamine, and (b) DSC results of Cu NPs synthesized using a solvothermal method.

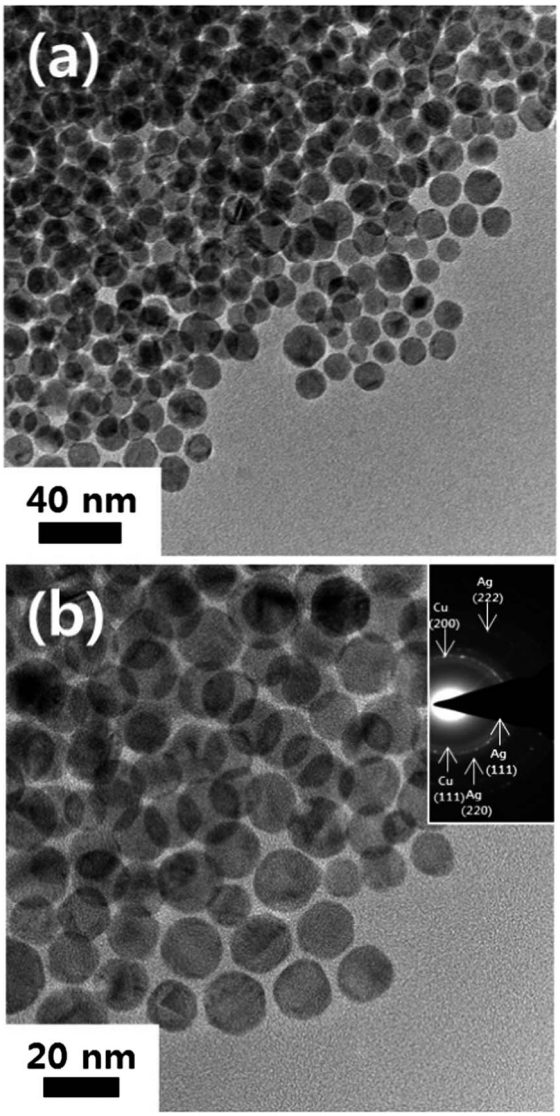


Fig. 5 TEM images of Cu@Ag core–shell NPs immersed at 80 °C for 2 h: (a) low-magnification and (b) high-magnification images with a SAED pattern (inset).

oxidation of Cu NPs. The total intensity of the Ag peaks increased with increasing immersion temperature, suggesting that the amount of Ag coating increased with results identical to those shown in Fig. 7. The main peak of the Ag coating shell was (200).

### 3.3. Anti-oxidation behavior of Cu@Ag nanoparticles

Based on the results shown in Fig. 5–8, the optimal Ag immersion coating condition was determined to be 150 °C for 2 h. High-temperature XRD was then carried out in order to analyze the anti-oxidation behavior of the Cu@Ag nanoparticles. The non-coated Cu NPs were also evaluated (Fig. 9) in order to compare their anti-oxidation behavior with that of the Cu@Ag NPs. The $Cu_2O(111)$ peak drastically increased at 150 °C in the non-coated Cu NPs, indicating that the oxidation initially emerged between 100 and 150 °C. It has been reported that Cu NPs synthesized using a polyvinyl pyrrolidone (PVP) capping agent 20–30 nm in size oxidized at 240 °C.[23] Thus, the size of Cu NPs and the capping agent used were expected to be the cause of the dissimilarity in the onset of oxidation. It is possible to produce high-quality Cu NPs using OA, but they are more vulnerable to oxidation than the PVP capping agent in air.[19,31]

We synthesized Cu NPs with an average size of 11.60 nm that had a higher surface energy than other Cu NPs several tens or hundreds of nanometers in size. Cu NPs synthesized in this manner are easily oxidized at lower temperatures. Meanwhile, the Cu(111) peak broadened up to 100 °C and became sharper when it approached 150 °C. This demonstrated that recrystallization mentioned in Fig. 4(b) and grain growth occurred with the Cu NPs. In addition, the Cu peak intensity decreased and the $Cu_2O$ peak intensity increased after reaching 200 °C. If the NPs are heated above 300 °C, they are expected to finally transform into CuO in order to achieve thermodynamic stability.[22,23]

Fig. 10 shows the high-temperature XRD patterns of Cu@Ag NPs immersed for 2 h at 80 and 150 °C. As shown in Fig. 10(a), the $Cu_2O(111)$ peak in the sample coated at 80 °C weakly appeared at 250 °C and significantly grew at 300 °C. Fig. 10(b)

 

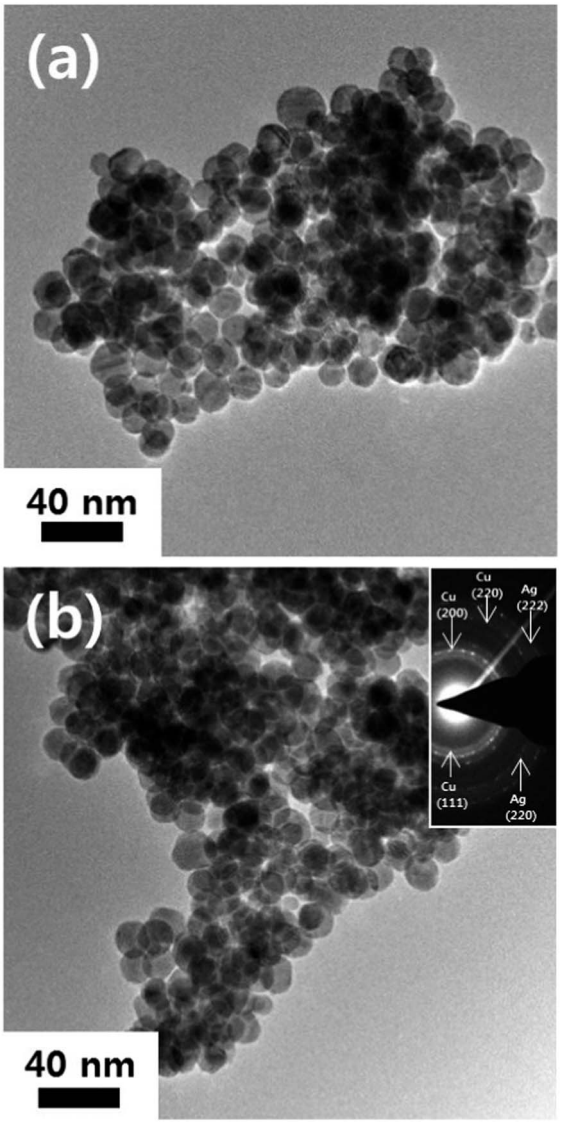


Fig. 6 TEM images of Cu@Ag core–shell NPs immersed for 2 h at (a) 130 °C and (b) 150 °C.

shows the sample coated at 150 °C. In this case, a $Cu_2O(111)$ peak did not emerge until 250 °C, and it grew slightly at 300 °C. These results mean that the anti-oxidation property was improved with the existence of the Ag shell and increased the immersion coating temperature because of the enhanced average Ag shell thickness and density.

# 4. Discussion

## 4.1. Size distribution of nanoparticles synthesized using varying temperatures

The change in the size of the Cu NPs shown in Fig. 1 can be explained using theoretical considerations of nucleation and growth. It has been reported that the nucleation and growth of NPs can be interpreted using La Mer's model,[31,32] which is mainly influenced by the cycle of supplied atoms. According to La Mer's model, primary NPs are nucleated when the concentration of atoms reaches a critical supersaturation ($C_{crit}$) level, followed by growth after a drop in the concentration below the $C_{crit}$ level. The atoms, supplied by the reduction reaction, are almost consumed by the nucleation and growth steps.

Ostwald ripening is another important growth mechanism of NPs;[32] however, ripening is difficult in NPs surrounded by a capping agent. If the nucleation quickly bursts because of vigorous reduction, the concentration of metallic atoms decreases rapidly. The growth caused by the supply of atoms slows because the remaining metal atoms are scarce. In order to synthesize fine and uniform NPs, atoms should be sufficiently and rapidly consumed at the $C_{crit}$ level. If there is only slight nucleation, the resultant concentration drop is also weak and the nucleation and growth step will be repetitive. This situation induces a substantial variation in particle size whose nucleation and growth depends on the supply time of atoms.

Fundamentally, the number of Cu atoms supplied would depend on the reaction temperature. At the relatively low temperature of 230 °C, atoms are slowly added until reaching the $C_{crit}$ level and nucleation is weak. Hence the atom concentration will be close to the $C_{crit}$ level during NP formation. A prolonged nucleation time and a chance for sufficient growth can cause the significant size deviation observed in Fig. 1(a). Meanwhile, the reduction and nucleation rates at 240 °C slightly accelerated, causing a reduction in the size deviation. However, the average size is much larger than that of NPs synthesized at 250 °C, the temperature at which the nucleation rate is maximized. Synthesis at 250 °C induces burst nucleation and results in the formation of extremely fine NPs. After the burst, the remaining number of atoms that could be used in the subsequent growth will decrease significantly.

## 4.2. Analysis of the Cu nanoparticle synthesis mechanism using varying reaction times

The NP morphologies changed with increased reaction time, as shown in Fig. 2. Interestingly, the polyhedral NPs, which were initially smaller than 10 nm, gradually increased to 30 nm in 15 min. After that point, the size of the NPs decreased as they became spherical.

This behavior is similar to that of synthesized Au NPs reported by many research groups.[33–35] When a solution containing Au NPs is heated to a specific temperature, larger NPs transform into smaller spherical NPs using particular ligands, including amines, silanes, and phosphines. This phenomenon is called the digestive-ripening process;[33] however, the mechanisms for this behavior have not been definitively clarified. Nevertheless, it has been reported that the particular ligand causes dissolution behavior to occur on the active surface sites (edges or corners) of large NPs, followed by a reprecipitation process.[34] Reprecipitated NPs form as smaller and more spherical NPs, resulting in enhanced monodispersion.[34] Prasad *et al.* reported that larger (<50 nm) Au NPs became smaller (2–6 nm) when using alkanethiol ligands.[35] They also reported similar behavior in other metal NPs when suitable ligands were used. We synthesized NPs using OA structured by an amine ligand. We expected that digestive-ripening behavior would

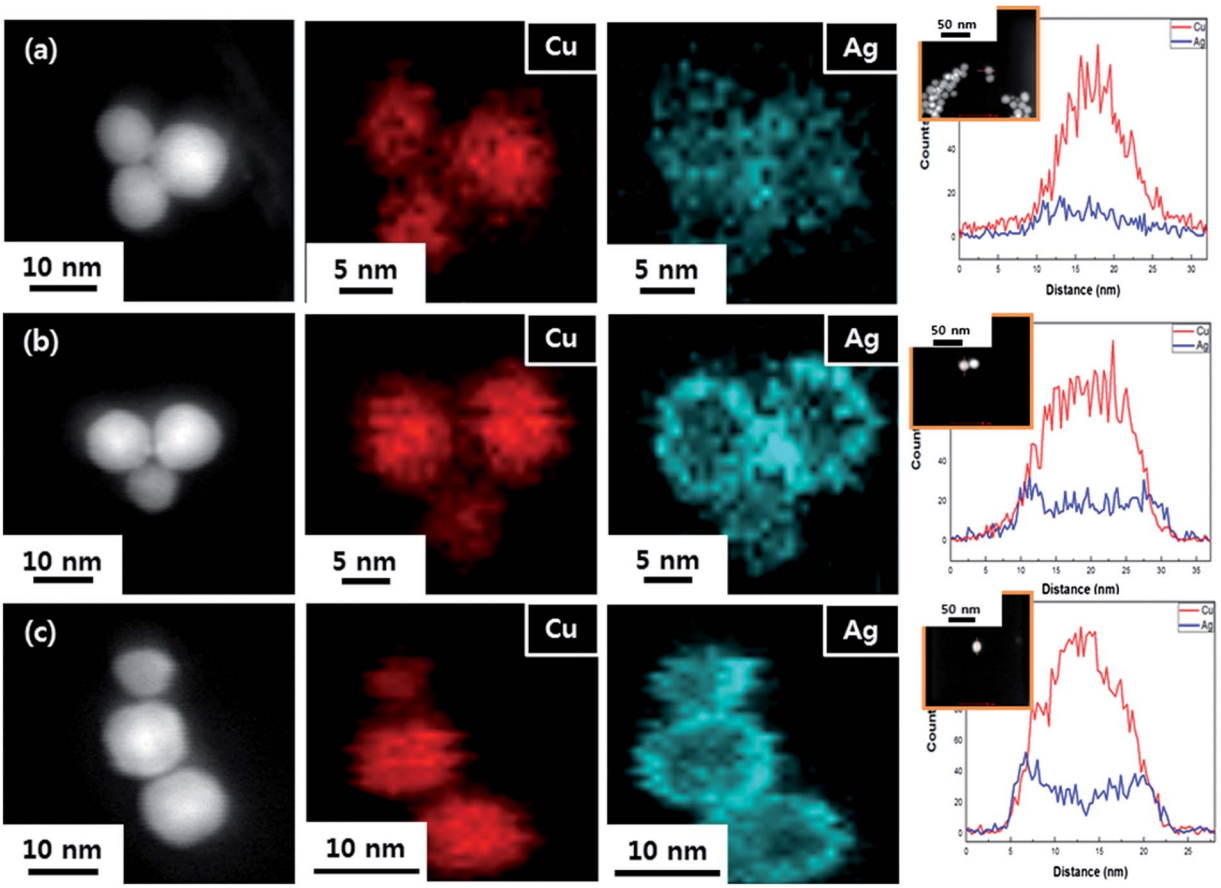


Fig. 7 Elemental mapping and line profile images of Cu@Ag NPs synthesized with different reaction temperatures for 2 h: (a) 80, (b) 130, and (c) 150 °C.

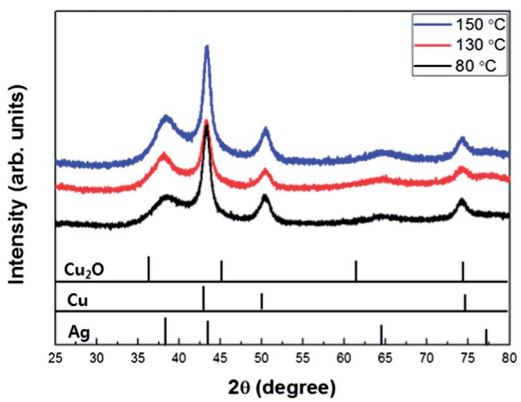


Fig. 8 XRD patterns of Cu@Ag NPs coated for 2 h at 80, 130, and 150 °C.

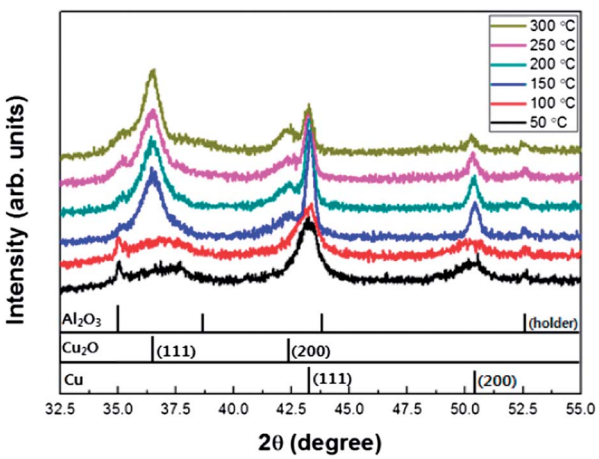


Fig. 9 High-temperature XRD patterns of Cu NPs synthesized for 3 h at 240 °C.

arise after 15 min and that spherical NPs would form. The digestive-ripening behavior in our synthesis phase was relevant to the transformation from $Cu_2O$ to Cu (Fig. 3).

### 4.3. Characterization of the Ag shell as a function of immersion temperature

The Ag shell quality was enhanced with increased immersion temperature, as presented in Fig. 7, 8, and 10. Other interesting results, excluding the anti-oxidation property, were observed in Fig. 10. In the case of the Ag(200) peak shown in Fig. 10(a), the intensity gradually became weaker; however, the sharpness was slightly enhanced as the temperature increased. Meanwhile, the intensity of the Ag(111) peak increased during heating. However, the Ag(200) peak of the sample immersed at 150 °C

 

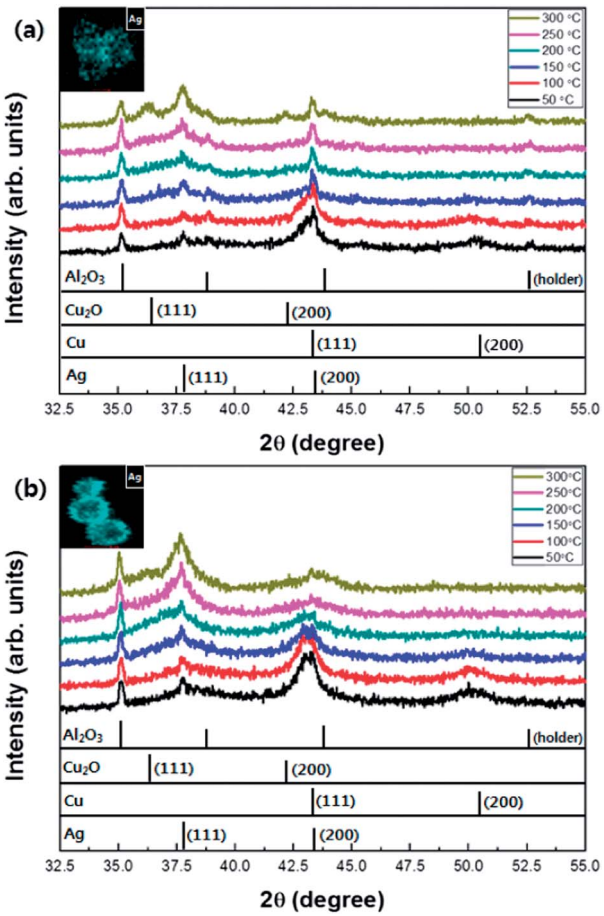


Fig. 10 High-temperature XRD patterns of Cu@Ag NPs coated at (a) 80 °C and (b) 150 °C with elemental mapping images of the Ag shell (inset).

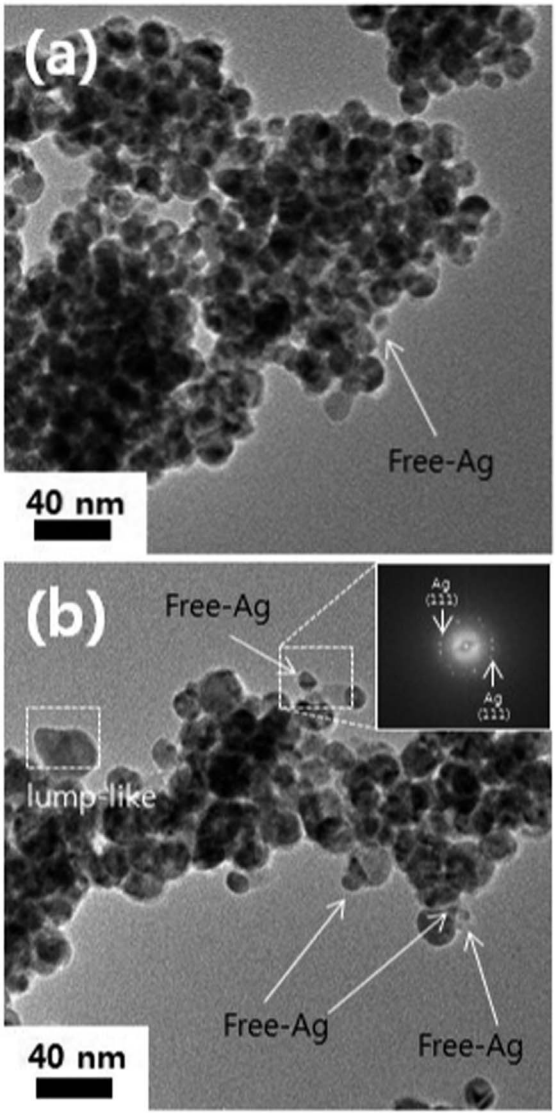


Fig. 11 TEM images of Cu@AgNPs immersed at (a) 80 °C and (b) 150 °C after annealing at 200 °C for 15 min.

[Fig. 10(b)] became broader and weaker with the growth of the Ag(111) peak with increasing temperature, especially from 200 °C.

The Ag-coated Cu structure exhibits considerable lattice mismatch (approximately 11%) and a positive enthalpy of mixing (104 meV per atom at 50 at% Cu), causing an unstable interfacial energy.[19] Hence the Ag atoms were segregated to decrease the interfacial energy on the Cu surface during heating, forming free Ag NPs.[19] This phenomenon can be considered as the final state of Ag dewetting. This is a spontaneous reaction mainly caused by surface diffusion, which can be accelerated when the Ag layer is structurally dense as compared to a sparse structure with voids. The Ag shell was extremely porous in the sample immersed at 80 °C, as shown in Fig. 7(a). Annealing above 150 °C mainly caused enhanced crystallinity and grain growth in the Ag shell, as well as slight dewetting due to reduced long-distance diffusion in the sparse structure. As a result, the number of free Ag NPs in the sample is relatively low [Fig. 11(a)]. As compared with Fig. 10, it is inferred that the slight decrease of Ag(200) peak intensity is related to thickness reduction by the dewetting behavior and the increase of the Ag(111) peak intensity is related to the formation of free Ag, respectively. In other words, the increased intensity of the Ag(111) peak is linked closely to the increased number of free Ag. The sharpness of the Ag(200) peak was due to the enhanced crystallinity and grain growth of the Ag shell. In the case of the sample immersed at 150 °C, Ag dewetting was dominant owing to the dense shell structure, which favors diffusion, forming a large number of free Ag NPs [Fig. 11(b)]. As a result, the Ag(200) peak became broader and weaker with the faster increase of Ag(111) peak intensity shown in Fig. 10(b). The broadening result in the XRD peak stemmed from the nature of the extremely thin Ag coating layer as a function of the dewetting. In an earlier report, the effects of the sintering process on Cu@Ag NPs were presented, demonstrating that the surface diffusion rate also changed with varying Ag shell thicknesses.[36] To confirm the abovementioned discussion, we examined the Ag layers of the samples formed at 80 and 150 °C and annealed at 200 °C for 15 min using TEM, and the results are presented in Fig. 11. Free Ag NPs in Ag layers formed at 80 °C were not observed except for

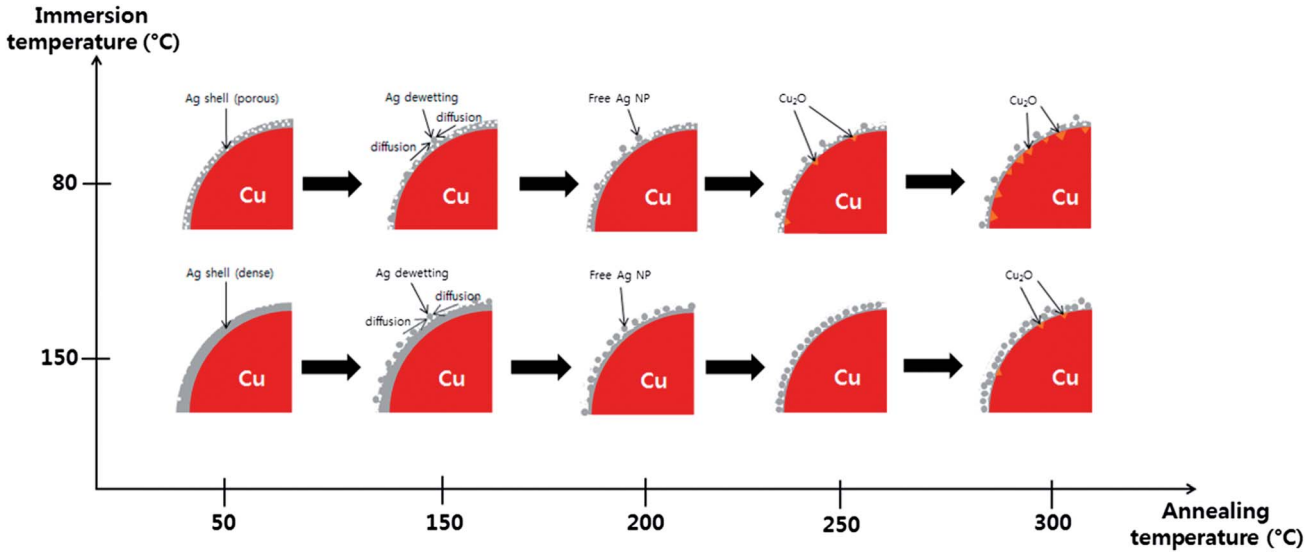


Fig. 12 Schematic images of the Ag dewetting mechanism in ultrafine Cu@Ag NPs immersed at 80 and 150 °C during annealing.

an NP near the center shown in Fig. 11(a). However, the free Ag NPs were observed more frequently in Ag layers formed at 150 °C [Fig. 11(b)], which induced both the Ag(111) peak growth and Ag(200) peak broadening [Fig. 10(b)]. In particular, novel lump-like nanostructures were also found along with the established spherical NPs, suggesting another result of Ag dewetting. Dewetted Ag might form the lump-like structures, followed by the formation of free Ag NPs detached from the Cu@Ag NP surface. It is noteworthy that oxidation did not occur if the Ag coating remained adequately thick despite the formation of lump-like structures or free Ag NPs caused by Ag dewetting. This is the reason why anti-oxidation is maintained at higher temperatures even with Ag layers formed at 150 °C. There have been many reports regarding the Ag dewetting behavior in Cu@Ag NPs. These reports indicated that oxidation occurred when pure Cu was exposed by Ag dewetting.[23,24,27] However, we explain the oxidation behavior with respect to the quality of the Ag shell.

Fig. 12 shows schematic images of the slightly different Cu@Ag NP oxidation mechanisms from NPs formed through immersion at 80 and 150 °C. Rapid oxidation occurred in the Ag shell formed at 80 °C because of its exposed porous microstructure. First, slight Ag dewetting occurs on specific active sites on the Ag shell having a low diffusion rate. As this behavior accelerates from 200 °C, free Ag NPs detach from the surface of Cu NPs due to the unstable interfacial energy. Finally, oxidation is induced on the Cu surface coated with the thinnest Ag layer from 250 °C. The Ag shell was thick and dense in the sample immersed at 150 °C. Thus, the time required for oxygen atoms to meet the Cu surface will be longer than that of the sample immersed at 80 °C, although the diffusion rate of the Ag atoms is faster and a greater number of free Ag NPs are thus generated. Consequently, it takes more time to cause oxidation in a thick and dense Ag shell, as indicated by the initiation of oxidation near 300 °C in Fig. 10(b). Considering the density of the Ag shell, oxidation is preferentially induced on the Cu surface coated with the thinnest Ag layer, which is generated by excessive Ag dewetting.

## 5. Conclusion

Cu@Ag NPs with an average diameter of 17 nm were synthesized using a solvothermal method and an immersion coating process and their oxidation behavior was analyzed. The Cu NP size distribution caused by varying the synthesis temperature could be explained using La Mer's model. The Cu NP synthesis mechanism as a function of increased reaction duration was determined to be the digestive-ripening process. During the synthesis at 240 °C, spherical NPs of a pure Cu phase were formed after 15 min. After increasing the immersion temperature to 150 °C, the average thickness and density of the Ag shell increased mainly as a result of enhanced activation. The sample immersed at 150 °C, even though it generated more free Ag NPs because of its dense structure, was evidently superior to the sample immersed at 80 °C in regards to the anti-oxidation property. Consequently, the anti-oxidation property of the Cu@Ag NPs was strongly dependent on the quality of the Ag shell.

## Acknowledgements

This study was financially supported by the National Research Foundation (NRF) of Korea funded by the Ministry of Education, Science and Technology (2011-0009088). The authors also thank Korean Basic Science Institute (KBSI) for the TEM, FT-IR, and XRD analyses.

## References

1 J. Liu, Y. H. Ahn, J.-Y. Park, K. H. Koh and S. Lee, *Nanotechnology*, 2009, **20**, 445203.
2 B.-L. Chen, H. Hu, Q.-D. Tai, N.-G. Zhang, F. Guo, B. Sebo, W. Liu, J.-K. Yuan, J.-B. Wang and X.-Z. Zhao, *Electrochim. Acta*, 2012, **59**, 581.
3 L.-C. Chen, C.-R. Ke and J.-M. Ting, *J. Electrochem. Soc.*, 2014, **161**, E28.

 

4 S.-B. Kang, Y.-J. Noh, S.-I. Na and H.-K. Kim, *Sol. Energy Mater. Sol. Cells*, 2014, **122**, 152.
5 M. Koo, K.-I. Park, S. H. Lee, M. Suh, D. Y. Jeon, J. W. Choi, K. Kang and K. J. Lee, *Nano Lett.*, 2012, **12**, 4810.
6 Z. Wang, N. Bramnik, S. Roy, G. D. Benedetto, J. L. Zunino III and S. Mitra, *J. Power Sources*, 2013, **237**, 210.
7 C. Kang, R. Baskaran, J. Hwang, B.-C. Ku and W. Choi, *Carbon*, 2014, **68**, 493.
8 B. Kang, J. Kno and M. Yang, *J. Micromech. Microeng.*, 2011, **21**, 075017.
9 S. H. Ko, H. Pan, C. P. Grigoropoulos, J. M. J. Fréchet, C. K. Luscombe and D. Poulikakos, *Appl. Phys. A: Mater. Sci. Process.*, 2008, **92**, 579.
10 L. Huang, Y. Huang, J. Liang, X. Wan and Y. Chen, *Nano. Res.*, 2011, **4**, 675.
11 L. Yang, A. Rida, R. Vyas and M. M. Tentzeris, *IEEE Trans. Microwave Theory Tech.*, 2007, **55**, 2894.
12 R. Sangoi, C. G. Smith, M. D. Seymour, J. N. Venkataraman, D. M. Clark, M. L. Kleper and B. E. Kahn, *J. Dispersion Sci. Technol.*, 2005, **25**, 513.
13 X.-F. Tang, Z.-G. Yang and W.-J. Wang, *Colloids Surf., A*, 2010, **360**, 99.
14 C. H. Kim and Y. Lee, *International Journal of Precision Engineering and Manufacturing*, 2011, **12**, 161.
15 W. Shen, X. Zhang, Q. Huang, Q. Xu and W. Song, *Nanoscale*, 2014, **6**, 1622.
16 S. Jeong, S. H. Lee, Y. Jo, S. S. Lee, Y.-H. Seo, B. W. Ahn, G. Kim, G.-E. Jang, J.-U. Park, B.-H. Ryu and Y. Choi, *J. Mater. Chem. C*, 2013, **1**, 2704.
17 W. Li, M. Chen, J. Wei, W. Li and C. You, *J. Nanopart. Res.*, 2013, **15**, 1949.
18 H. Jiang, K.-S. Moon and C. P. Wong, *Proc. -Int. Symp. Adv. Packag. Mater.*, Beckman center, Irvine, CA, March, 2005.
19 A. Muzikansky, P. Nanikashvili, J. Grinblat and D. Zitoun, *J. Phys. Chem. C*, 2013, **117**, 3093.
20 M. Grouchko, A. Kamyshny and S. Magdassi, *J. Mater. Chem.*, 2009, **117**, 3057.
21 M. Tsuji, S. Hikino, Y. Sano and M. Horigome, *Chem. Lett.*, 2009, **38**, 518.
22 H. T. Hai, H. Takamura and J. Koike, *J. Alloys Compd.*, 2013, **564**, 71.
23 C.-H. Tsai, S.-Y. Chen, J.-M. Song, I.-G. Chen and H.-Y. Lee, *Corros. Sci.*, 2013, **74**, 123.
24 H. T. Hai, J. G. Ahn, D. J. Kim, J. R. Lee, H. S. Chung and C. O. Kim, *Surf. Coat. Technol.*, 2006, **201**, 3788.
25 V. Mancier, C. Rousse-Bertrand, J. Dille, J. Michel and P. Fricoteaux, *Ultrason. Sonochem.*, 2010, **17**, 690.
26 M. Salvati-Niasari, Z. Fereshteh and F. Davar, *Polyhedron*, 2009, **28**, 126.
27 M. Chen, Y.-G. Feng, X. Wang, T.-C. Li, J.-Y. Zhang and D.-J. Qian, *Langmuir*, 2007, **23**, 5296.
28 M. Salavati-Niasari, N. Mir and F. Davar, *Appl. Surf. Sci.*, 2010, **256**, 4003.
29 C. S. Choi, Y. H. Jo, M. G. Kim and H. M. Lee, *Nanotechnology*, 2012, **23**, 065601.
30 I. Jung, K. Shin, N. R. Kim and H. M. Lee, *J. Mater. Chem. C*, 2013, **1**, 1855.
31 B. K. Park, S. Jeong, D. Kim, J. Moon, S. Lim and J. S. Kim, *J. Colloid Interface Sci.*, 2007, **311**, 417.
32 S. I. Cha, C. B. Mo, K. T. Kim, Y. J. Jeong and S. H. Hong, *J. Mater. Res.*, 2006, **21**, 2371.
33 J. Park, J. Joo, S. G. Kwon, Y. Jang and T. Hyeon, *Angew. Chem., Int. Ed.*, 2007, **46**, 4630.
34 S. Stoeva, K. J. Klabunde, C. M. Sorensen and L. Dragieva, *J. Am. Chem. Soc.*, 2002, **124**, 2305.
35 B. L. Prasad, S. I. Stoeva, C. M. Sorensen and K. J. Klabunde, *Langmuir*, 2002, **18**, 7515.
36 S. J. Kim, E. A. Stach and C. A. Handwerker, *Appl. Phys. Lett.*, 2010, **96**, 144101.